The electronic structure of $KNbO_3$: an XPS and XAS study

1994 J. Phys.: Condens. Matter 6 5039

(http://iopscience.iop.org/0953-8984/6/27/013)

J. Phys.: Condens. Matter 6 (1994) 5039–5052. Printed in the UK

The electronic structure of $KNbO_3$: an XPS and XAS study

L Douillard†, F Jollet†, C Bellin†, M Gautier† and J P Duraud‡

† CEA—CE Saclay—DSM/DRECAM/SRSIM, 91191 Gif sur Yvette Cédex, France
‡ Laboratoire Pierre Süe—CEA CNRS, 91191 Gif sur Yvette Cédex, France

Received 21 February 1994, in final form 8 April 1994

Abstract. The electronic structure of orthorhombic potassium niobate has been studied with a particular focus on empty electronic states. Occupied electronic states were analysed by x-ray photoelectron spectroscopy. Empty electronic states were probed by x-ray absorption spectroscopy at the oxygen K edge (531 eV), the niobium L_1 (2698 eV), L_2 (2465 eV), and L_3 (2371 eV) edges, and the potassium K (3608 eV) edge. Absorption experiments are interpreted in terms of orbital hybridizations using self-consistent tight-binding calculations. O K-edge structures are related to hybridizations of O 2p orbitals with Nb 4d, 5p, and 5s orbitals respectively. Nb L edges reflect the (t_{2g}, e_g) degeneracy lift of Nb 4d orbitals placed in the NbO_6 environment. The delocalization of Nb 4d e_g states is not found to be significantly larger than the delocalization of Nb t_{2g} states.

1. Introduction

Ferroelectric materials with the perovskite structure ABO_3 are of great interest in modern technology [1], as supports for binary memory devices, light modulators for optical communication systems, or pyroelectric detectors of radiation. Among such perovskite oxides, potassium niobate presents attractive properties for electro-optical and catalytic applications [2]. Physical and chemical properties of solids are related to a fundamental basic description, such as electronic structure. As a matter of fact, in the past few years, understanding of electronic structure has become sufficient to describe numerous properties of solids [13]. The present work deals with a description of the $KNbO_3$ electronic structure. Since the first x-ray photoelectron spectroscopy (XPS) investigations by Pertosa and Michel-Calendini [3], $KNbO_3$ has been the subject of many papers [4–6], dealing mostly with occupied electronic band structure. This work focuses on electronic empty states. While numerous authors deal with $KNbO_3$ occupied states, few works have been published on empty states [4, 5, 7].

Experimentally, the density of occupied states is probed using XPS, while local projected empty states are obtained by x-ray absorption spectroscopy (XAS) experiments, at the oxygen, niobium and potassium edges. Experimental results are qualitatively interpreted by comparison with self-consistent tight-binding calculations, performed for the cubic phase of $KNbO_3$.

Section 2 is devoted to sample preparation, experiments, and results. Section 3 deals with tight-binding calculations of the electronic band structure. Comparison between experimental and theoretical works is discussed in section 4. $KNbO_3$ x-ray absorption near-edge structure (XANES) spectra at O K and Nb L edges are interpreted in terms of orbital hybridizations.

0953-8984/94/275039+14$19.50

2. Experimental details and results

2.1. Samples

At room temperature (RT), the ferroelectric $KNbO_3$ structure, based on an NbO_6 octahedral framework, exhibits a slight distortion with respect to the ideal cubic perovskite structure. As determined by Hewat [8], the RT lattice is orthorhombic with parameters $a = 3.973$ Å, $b = 5.695$ Å and $c = 5.721$ Å at 22 °C. The space group is $Amm2$. The orthorhombic cell contains two $KNbO_3$ units. The polarization axis is parallel to [001]. $KNbO_3$ is an insulator with an optical band gap [9] around 3.5 eV.

Monocrystals of $KNbO_3$ were synthesized by the flux method (flux K_2O). Samples of thickness 0.5 mm were cut and mechanically polished, then annealed for 1 h at 750 °C in air to restore surface stoichiometry and remove carbon contamination.

2.2. XPS experiments

XPS was used to control sample stoichiometry and surface cleanliness. XPS spectra were recorded at room temperature on an Escalab VG Mark II spectrometer, using monochromatized Al Kα radiation ($h\nu = 1486.6$ eV). A flood-gun device (VG LEG 51) was used to reduce the charge phenomena occurring on the $KNbO_3$ samples under the photon beam. Nevertheless, according to the O 1s shift, a residual charge of about 1 eV was observed during XPS experiments.

Figure 1 displays a global XPS spectrum over 700 eV. Figure 2 shows XPS structures for binding energies ranging from about 45 eV up to the valence band. No noticeable C contamination is visible. The relative core-level binding energies are reported in table 1, using the O 1s line (fixed at 531 eV) as a reference. Our XPS measurements are in agreement with previous XPS studies [3].

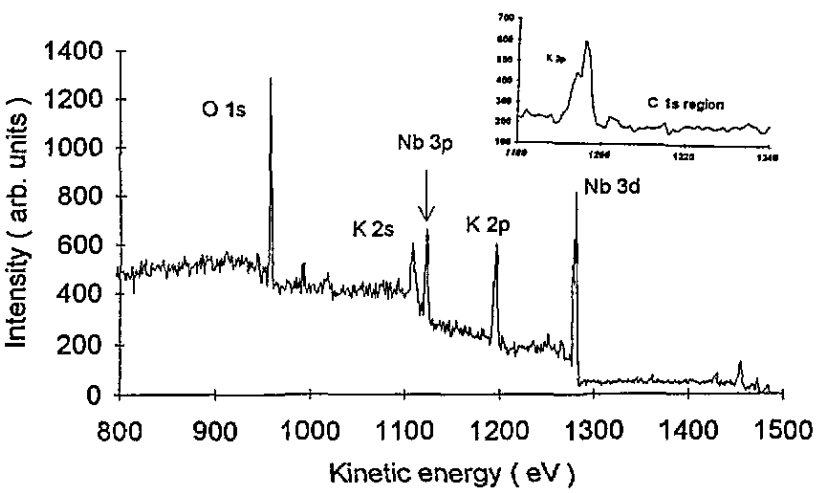

Figure 1. A global XPS spectrum of a $KNbO_3$ monocrystal. The axis label is kinetic energy. The x-ray source is a monochromatized Al Kα (1486.6 eV) source. A flood-gun device was used to reduce the charging effect.

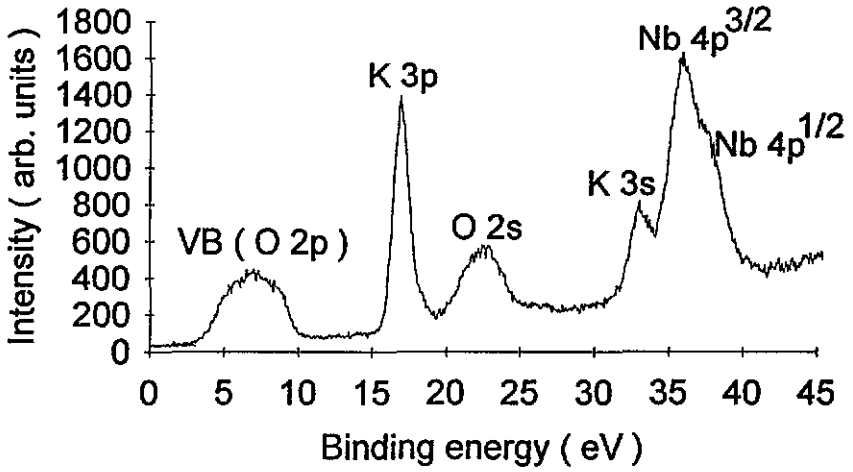

Figure 2. The XPS spectrum of an orthorhombic $KNbO_3$ monocrystal in the [50 eV, 0 eV] binding-energy range (the energy reference is the O 1s binding energy, fixed at 531.0 eV). The axis label is binding energy. The x-ray source is a monochromatized Al Kα (1486.6 eV) source. A flood-gun device was used to reduce the charging effect.

Table 1. XPS binding energies relative to O 1s taken at 531.0 eV for orthorhombic $KNbO_3$.

	K 3p	O 2s	K 3s	Nb $4p^{3/2}$	Nb $4p^{1/2}$	O 1s
Energy (eV)	16.9	22.5	33.1	35.9	37.3	531.0

2.3. XAS experiments

2.3.1. Method. When an atom absorbs an x-ray photon, electrons are emitted by the photoelectric effect. XANES deals with photoelectrons promoted in the first empty electronic states allowed by the dipole selection rules: $\Delta l = \pm 1$ and $\Delta s = 0$, where l and s represent the orbital momentum quantum number and spin quantum number respectively (transition $s \rightarrow p$ for K and L_1 edges and mainly $p \rightarrow d$ for $L_{2,3}$ edges). As demonstrated by Müller and Wilkins [10], a XANES spectrum is understandable as a product between the projected density of states of the absorbing atom, determined by the core-orbital symmetry and the dipole selection rules, and a matrix element. This description was established for metals, where the core-hole potential is fully screened by the valence electrons. As discussed in section 3, the validity of the latter hypothesis for insulator materials is questionable.

XANES experiments were carried out on the SU7 beam line for the O K edge (531 eV) and on the SA 32 beam line for the Nb L_1 (2698 eV), L_2 (2465 eV), and L_3 edges (2371 eV) and the K K-edge (3608 eV) at the Super-ACO synchrotron radiation facilities (LURE, Orsay). The O K-edge spectra were recorded by detecting the total electron yield. A flood-gun system was used in order to overcome the charge phenomena always observed on such insulating oxides. The energy resolution was 0.5 eV. For Nb and K edges, an absorbed-current detection method was used. The resolution was equal to about 0.8 eV. The ratio I/I_0, i.e. detected current (I) over incident beam intensity (I_0) was plotted as a function of photon energy E, yielding the absorption coefficient $\mu(E)$ [11].

Synchrotron radiation is a linearly polarized x-ray radiation. When working with monocrystalline samples, one has to consider the influence of the angle between the beam

and the sample normal on the XANES structures. Therefore XANES spectra were recorded at the magic angle so as to average polarization effects [12].

2.3.2. O K-edge spectra. According to dipole selection rules, O K-edge experiments probed the empty O *n*p density of states (O 1s → O *n*p transitions).

In a first approach, seven main structures can be distinguished on the O K-edge spectrum over the XANES domain. These structures are labelled A–G in figure 3. Structure energies are reported in table 2.

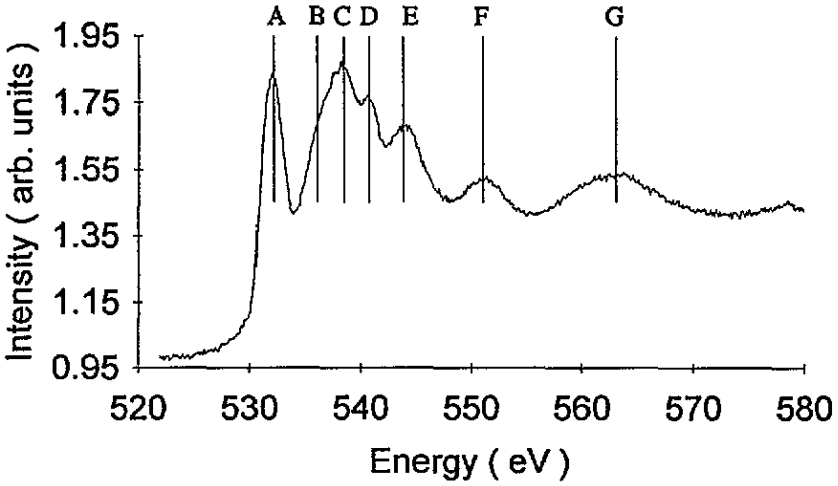

Figure 3. O K-edge (531 eV) XANES spectrum of an orthorhombic $KNbO_3$ monocrystal recorded at the magic angle. The spectra were recorded using the total electron yield.

Table 2. XANES O K-edge structure energies for orthorhombic $KNbO_3$. The XANES spectrum was recorded at the magic angle.

	E_0	A	B	C	D	E	F	G
Energy (eV)	530.8	532.1	536.0	538.4	540.7	543.8	551.0	563.0

2.3.3. Nb L_1-edge spectra. Nb L_1 XANES spectra correspond to Nb 2*s* → Nb *n*p transitions and therefore probed the partial Nb *n*p density of states. The Nb L_1 (2698 eV) XANES spectrum (figure 4(*a*)) exhibits mainly three structures within the first 50 eV. These structures are labelled A, B, and C in figure 4(*a*). Two other smooth structures are also visible around 2735.5 eV (D) and 2742.5 eV (E) (see table 3).

Table 3. XANES Nb L_1-edge structure energies for orthorhombic $KNbO_3$. The XANES spectrum was recorded at the magic angle.

	E_0	A	B	C	D	E
Energy (eV)	2698.2	2702.0	2714.8	2726.0	2735.5	2742.5

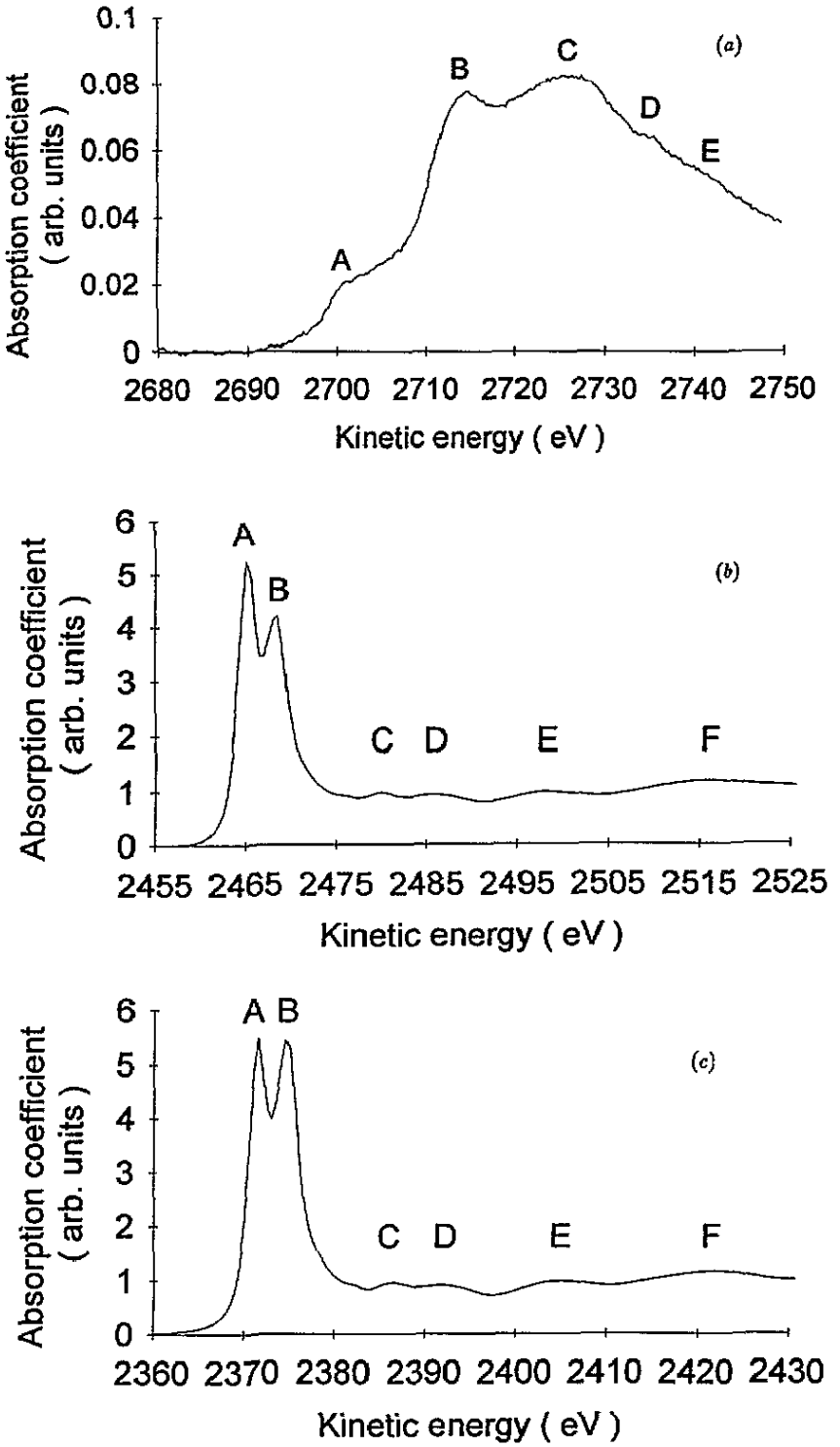

Figure 4. Nb L edges of an orthorhombic $KNbO_3$ monocrystal recorded at the magic angle. The spectra were recorded using the current absorption. (*a*) The Nb L_1 (2698 eV) XANES spectrum; (*b*) the Nb L_2 (2465 eV) XANES spectrum; (*c*) the Nb L_3 (2371 eV) XANES spectrum.

2.3.4. Niobium L_2- and L_3-edge spectra. For the L edge, dipole-allowed excitations of 2p electrons give two white lines, L_2 and L_3. These two white lines correspond to the ways in which the spin number s can couple to the orbital momentum number l to give authorized total momentum number $j = l \pm s$. As a matter of fact, when considering spin–orbit coupling, the dipole selection rules become $\Delta j = 0, \pm 1$ giving two L edges; the L_2 edge, corresponding to $2p^{1/2} \rightarrow nd$ transitions, and the L_3 edge, corresponding to $2p^{3/2} \rightarrow nd$ transitions. The (L_2, L_3) energy separation is defined by the spin–orbit coupling and, for a pure atomic multiplet spectrum, the theoretical (L_3/L_2) intensity ratio is two.

Both XANES regions, Nb L_2 (2465 eV) (figure 4(*b*)) and Nb L_3 edges (2371 eV) (figure 4(*c*)), present a double white line (A, B), followed by four noticeable structures (C, D, E, F). Peak positions are reported in table 4. The energy separation between the Nb L_2 and L_3 edges, that is, the spin–orbit splitting, is $E_0(L_2) - E_0(L_3) = 93.5$ eV, where E_0 designates the edge energy determined by the inflexion point method. The L_3/L_2 white-line intensity ratio, measured in the range ($E_0 - 5$ eV, $E_0 + 10$ eV) is 1.5. Note that L_2 ($2p^{1/2}$) and L_3 ($2p^{3/2}$) Nb edges differ also in the relative intensities of the two structures involved in the white line. Estimations of these relative intensity ratios give $L_2A/L_2B = 1.3$, $L_3A/L_3B = 1.0$. Estimates of both types of relative intensity ratio were obtained after a linear extrapolation and subtraction of the background contribution.

Table 4. XANES Nb L_2- and Nb L_3-edge structure energies for orthorhombic $KNbO_3$. The XANES spectra were recorded at the magic angle.

	E_0	A	B	C	D	E	F
Nb L_2 (eV)	2464.0	2465.1	2468.3	2480.1	2486.0	2498.1	2516.5
Nb L_3 (eV)	2370.5	2371.4	2374.5	2386.5	2391.8	2405.1	2422.1

2.3.5. K K-edge spectra. The K K-edge (3608.4 eV) XANES spectrum, related to the partial K np density of states, is displayed in figure 5. It shows mainly five structures, whose energy positions are reported in table 5.

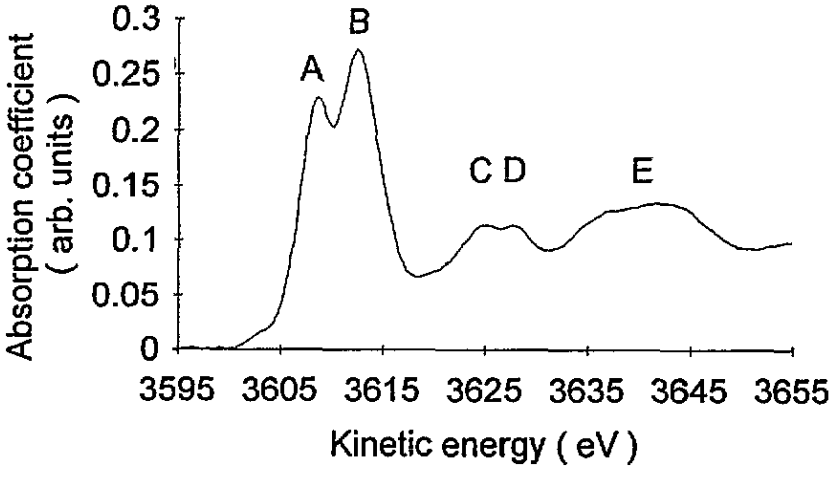

Figure 5. The K K-edge (3608 eV) XANES spectrum of an orthorhombic $KNbO_3$ monocrystal recorded at the magic angle. The spectra were recorded using current absorption.

Table 5. XANES K K-edge structure energies for orthorhombic $KNbO_3$. The XANES spectrum was recorded at the magic angle.

	E_0	A	B	C	D	E
Energy (eV)	3607.3	3608.5	3612.3	3624.8	3627.5	3640.5

Interpretations of the XANES spectra will be discussed in section 4.

3. Density of states calculations

Electronic densities of states (DOS) are calculated using a self-consistent semi-empirical tight-binding method [13, 14]. The tight-binding method is very flexible and allows an easy projection of the DOS on particular atomic sites and/or particular angular momenta. A short description of the tight-binding method follows. For more details about the method, we refer to the works cited above.

3.1. The tight-binding method

One consider that atoms, constituting the solid, are composed of an ionic core (nucleus + core electrons) and valence electrons. A set of n_k atomic orbitals is associated with each atom k. The atomic orbital basis is assumed to be an orthogonalized basis (complete neglect of differential overlap approximation). Monoelectronic wave functions φ_i are developed as a linear combination of atomic orbitals $|kj\rangle$ (k atom, j orbital)

$$\varphi_i = \sum_k \sum_j a^i_{kj} |kj\rangle.$$

These monoelectronic wave functions are used to build a Slater determinant φ. By solving the Schrödinger equation $H\varphi = E\varphi$, within the Hartree–Fock approximation, monoelectronic wave functions φ_i, that is, $a^i_{j,k}$ terms and corresponding eigenvalues E_i, are determined. The number of electrons on each atom is then evaluated and the calculation is iterated with the final charges used as new initial charges until self-consistency is achieved.

The Hamiltonian operator H is built up as follows. Hamiltonian diagonal terms depend on atomic orbital energies, the mean intra-atomic electron–electron repulsion of atom k (U_k parameters), the Madelung potential on each atom k, and crystal-field terms. The crystal-field terms take into account the symmetry of the transition-metal environment. In the case of cubic $KNbO_3$, the Nb atom has a pure octahedral O environment NbO_6 and the crystal-field influence induces a degeneracy lift of the 4d orbitals in (t_{2g}, e_g) sets.

Hamiltonian off-diagonal terms consist of diatomic hopping terms between orbital j on atom k $|kj\rangle$ and orbital j' on atom k' $|k'j'\rangle$. The hopping terms [13] are calculated by Slater–Koster equations [15]. They take into account the relative geometry of the orbitals $|kj\rangle$ and $|k'j'\rangle$, and terms $V_{jj'l}$. $V_{jj'l}$ terms are functions of the distance R between atoms k and k' and $\eta_{jj'l}$, an adjustable tight-binding parameter depending on the solid structure. For the nearest neighbours, these $V_{jj'l}$ terms are calculated according to Harrison's formula [13]. For second-neighbour interactions, a modified $V_{jj'l}$ formula [16] is used.

The present tight-binding method is a monoelectronic method; that is, (electron–electron) correlations are neglected. Consequently, the tight-binding method seems not to be appropriate for electronic structure calculations of transition-metal oxides (*n*d cations), since d electrons are known to present important correlation effects. Nevertheless, work by

Jollet *et al* [17] on the Y_2O_3 system has shown that in the case of the formal d^0 cation (such as Nb in $KNbO_3$) correlation effects are weak and tight-binding DOS calculations are expected to be reliable.

Spin–orbit coupling is not considered. As a consequence tight-binding calculations do not distinguish L_2 from L_3 edges. Nevertheless, in a first approximation, L_2 and L_3 edges can be compared individually with the partial projected Nb 4d density of states. As for K edges, they are not affected by spin–orbit coupling ($l = 0$).

Another limitation deals with the (core-hole–electrons) interaction. In insulator materials, the core-hole potential on the absorbing atom is not fully screened by the valence electrons. When calculating electronic states, one has to take into account the influence of the core hole. The present first calculations do not take into account such an improvement. As a consequence, we do not expect more than a qualitative agreement between experimental XANES spectra and DOS calculations. Note, however, that the core-hole potential effects are less crucial for the O K edge, since valence electrons are preferentially O 2p electrons.

3.2. Computational details

At RT, orthorhombic $KNbO_3$ exhibits only a slight distortion with respect to the ideal cubic perovskite structure. Thus the $KNbO_3$ electronic structure was calculated in the ideal cubic perovskite structure, assuming similar band diagrams for both phases.

The monoelectronic wave functions of the $KNbO_3$ system are developed on an orthogonal basis of atomic orbitals including 2s and 2p orbitals for the O atoms, 4d, 5s, and 5p orbitals for the Nb atoms, and 3s and 3p orbitals for the K atoms. Occupied orbital energies and mean intra-atomic electron–electron parameters (U_k parameters) were initialized with values given by Harrison [13]. The energy of the unoccupied Nb orbital 5p was taken from Moore's table [18]. Diatomic hopping terms considered were Nb–O nearest neighbours and O–O and Nb–Nb second neighbours with respective r values 0.9 and 2.3. For relative ss, pp, sp, and pd diatomic hopping parameters $\eta_{jj'l}$, we again used Harrison's data [13]. Note that diatomic hopping terms involving K atoms were not considered (fixed to zero). During calculations K atoms keep an ionic charge equal to +1. Nevertheless, K atoms influence band-structure determination through the Madelung potential effect.

Such computational parameters (orbital energies, intra-atomic Coulomb repulsion parameters, diatomic hopping parameters) were slightly modified so as to fit the experimental data (XPS spectra, band gap, and XANES spectra). Adjusted parameters are reported in tables 6 and 7.

Table 6. Orbital energies (in electronvolts) used for cubic $KNbO_3$ DOS calculations [13, 18].

	O 2s	O 2p	Nb 4d	Nb 5s	Nb 5p	K 3p	K 3s
Initial value	−29.14	−14.13	−10.03 $r_D = 1.28$	−5.95	−3.32	−23.0	−4.19
Fitted value	−29.2	−15.2	−10.5 $r_D = 1.28$	−7.6	−7.4	−23.0	−4.2

Note that theoretical DOSs are broadened with a Gaussian shape with a 1 eV sigma parameter.

Table 7. Adjusted tight-binding parameters used for cubic $KNbO_3$ DOS calculations: diatomic hopping parameters η as defined by Harrison [13] and mean intra-atomic electron–electron Coulomb repulsion parameters as defined by Harrison [13] (U_k parameters).

	η							U_k parameters		
	s–s σ	s–p σ	p–p σ	p–p π	s–d σ	p–d σ	p–d π	U_O (eV)	U_{Nb} (eV)	U_K (eV)
Initial value	−1.320	+1.42	+2.22	−0.63	−3.160	−2.950	1.360	14.47	6.5	5.56
Fitted value	−1.350	+1.400	+1.500	−0.75	−2.900	−2.900	1.340	14.47	6.5	4.56

4. Theoretical results and discussion

4.1. Valence band

Determination of the electronic band structure of $KNbO_3$ has been the subject of many papers [4–6]. Previous efforts were essentially focused on occupied valence band (VB) states. According to reported studies, the VB DOS is dominated by O 2p orbitals with a contribution of Nb orbitals in the lower and middle parts of the VB. The present VB DOS calculations, reported in figure 6(*a*), are in agreement with such a description. The shape of the theoretical VB DOS exhibits two main structures (a, b), split by about 2.5 eV. The cubic $KNbO_3$ theoretical VB is about 6 eV wide, in good agreement with the experimental value. Note that a slight increase of theoretical VB width is expected for the orthorhombic phase [19]. More precisely, Nb 5s–O 2p orbital hybridizations take place preferentially in the lower part of the VB DOS, while Nb 4d and 5p both contribute mainly to the lower and middle parts. The present theoretical VB DOS shape is in reasonable agreement with OLCAO VB calculations performed by Yong-Nian Xu *et al* [5] and recent LMTO VB calculations reported by Neumann *et al* [6]. Taking into account photoionization cross sections allows direct comparison with experiments. In this case, a corrected DOS N_c is calculated through the following relation: $N_c(E) = \sum_i \sum_j \sigma_{ij}(E) N_{ij}(E)$, where $\sigma_{ij}(E)$ represents the photoionization cross section of orbitals of symmetry i of atom type j and $N_{ij}(E)$ the theoretical DOS of orbitals of symmetry i of atom type j at the same energy E. For XPS experiments, one has to consider a ratio [20] $\sigma_{Nb\ 4d}/\sigma_{O\ 2p} = 8.0$. This ratio becomes [21] 0.25 for UPS experiments. Figure 6(*b*) and (*c*) displays comparisons between experimental spectra and the associated N_c VB DOS for XPS and UPS respectively. For these two energy ranges, corrected VB DOS and experiments are in reasonable agreement, especially for the UPS VB. For the XPS VB the photoionization cross section ratio seems slightly too important.

4.2. Nb L_2 and L_3-edge XANES results

Nb L x-ray absorption experiments were carried out to probe the Nb 4d and Nb 5s conduction band (CB) states of orthorhombic $KNbO_3$. Note that, in practice, estimates of relative matrix elements [22] show that the p → d transitions dominate over the p → s transitions.

According to earlier studies [4, 5], the $KNbO_3$ CB is derived mostly from the Nb 4d orbitals. CB calculations generally agree to predict two separate structures, Nb 4d t_{2g} and Nb 4d e_g, due to a lift of degeneracy of the 4d orbitals of the Nb atom in the octahedral NbO_6 site. The present Nb 4d local DOS projections, reported in figure 7, agree with such a description. Nevertheless, previous CB computations by Castet-Mejean and Michel-Calendini [4] predict an Nb 4d e_g state with a significantly delocalized (about 7 eV) character. Here, Nb 4d t_{2g} and e_g exhibit a similar shape (no strong delocalization of e_g states). Only a small additional feature appears on the high-energy side of the Nb 4d e_g DOS. This additional structure is probably related to (Nb–Nb) second-neighbour hybridization states.

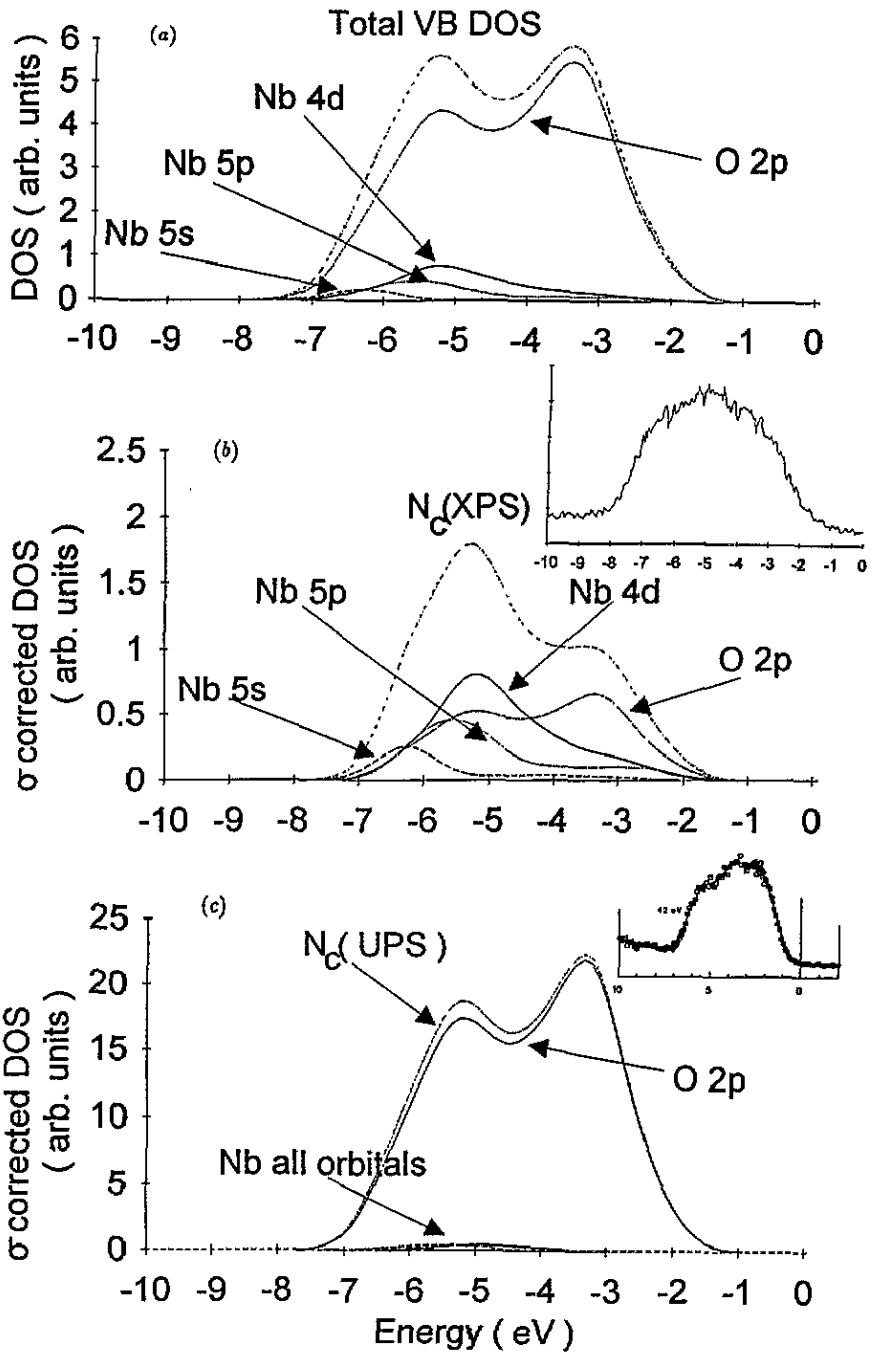

Figure 6. (*a*) The cubic $KNbO_3$ theoretical VB. The axis label is binding energy. (*b*) A comparison between the XPS VB spectrum and the related photoionization-cross-section-corrected VB calculations N_c(XPS) using [20] $\sigma_{Nb\ 4d}/\sigma_{O\ 2p} = 8.0$ (geometrical XPS spectrometer specifications are taken into account). The axis label is binding energy. (*c*) A comparison between the UPS VB spectrum (taken from [6]; the UPS spectrum has been obtained using synchrotron radiation and the photon energy is 42 eV) and the related photoionization-cross-section-corrected VB calculations N_c(UPS) using [21] $\sigma_{Nb\ 4d}/\sigma_{O\ 2p} = 0.25$. The axis label is binding energy.

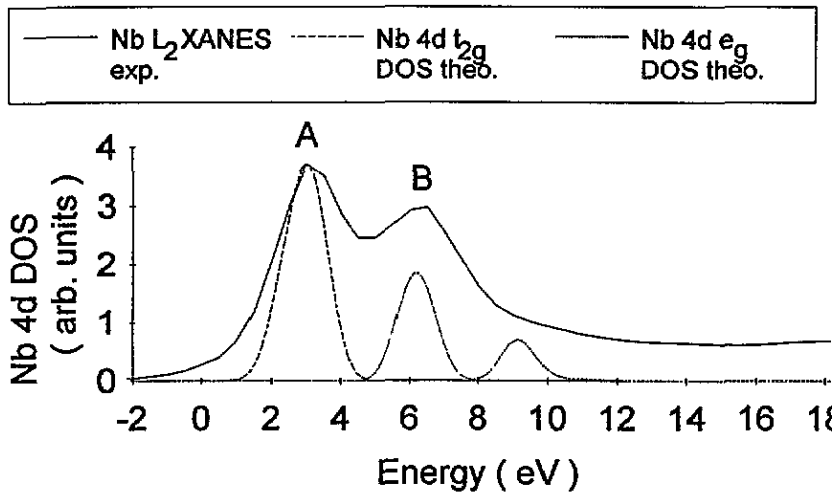

Figure 7. The Nb 4d theoretical DOS projection for cubic $KNbO_3$, in comparison with the experimental Nb L_2 XANES spectrum of orthorhombic $KNbO_3$.

When comparing the relative intensities of Nb 4d t_{2g} and Nb 4d e_g structures, we find serious discrepancies between XANES experiments and CB state calculations. Note that there is a change in the experimental relative intensities of Nb 4d t_{2g} and Nb 4d e_g when going from the Nb L_2 to the Nb L_3 edge. Such a modification is related to core-hole and p spin–orbit coupling effects. Since present computations do not take into account such improvements, no further attempt was made to reduce quantitative discrepancies between the theoretical Nb 4d DOS and Nb L_2 and L_3 XANES experiments.

More recently, Soldatov *et al* [7], relying on both theoretical and experimental studies, described the first 10 eV CB to be composed of four distinctive features. The present Nb L_2 and L_3 XANES spectra do not exhibit such a four-structure shape. Only two distinctive structures (A, B) are observed (figure 4). The experimental disagreement is difficult to explain. According to Soldatov *et al* [7], x-ray absorption experiments were recorded with an energy resolution of 0.2 eV. The present Nb L_3 XANES energy resolution is larger, about 0.8 eV. Nevertheless, we do not think that experimental disagreement lies exclusively in energy resolution differences. As no details are given by Soldatov *et al* [7] about sample preparation, we suggest a possible NbO_x contamination.

Thus both Nb L_2 and L_3 XAS experiments and tight-binding CB state calculations confirm the (t_{2g}, e_g) degeneracy lift of the Nb 4d orbitals. The experimental ligand-field value is 3.2 eV. The 10 Dq parameter used to fit the experiment is 2.3 eV, the difference being due to hopping terms. Furthermore, no strong delocalization of the Nb 4d e_g empty state is noticed.

4.3. O K-edge XANES results

The p empty states on the O atoms are the final states of a dipole transition from the O 1s atomic level (O K-edge absorption). The local O 2p DOS is displayed in figure 8. Using CB tight-binding calculations, the $KNbO_3$ O K-edge XANES structures can be qualitatively attributed over the first 10 eV. Note that, to make the physics clearer, a molecular orbital approach is used.

Structure A, centred at 532.1 eV (figure 3), is interpreted as an almost pure hybridization of O 2p with Nb 4d t_{2g} orbitals, through a π^* interaction (anti-bonding state).

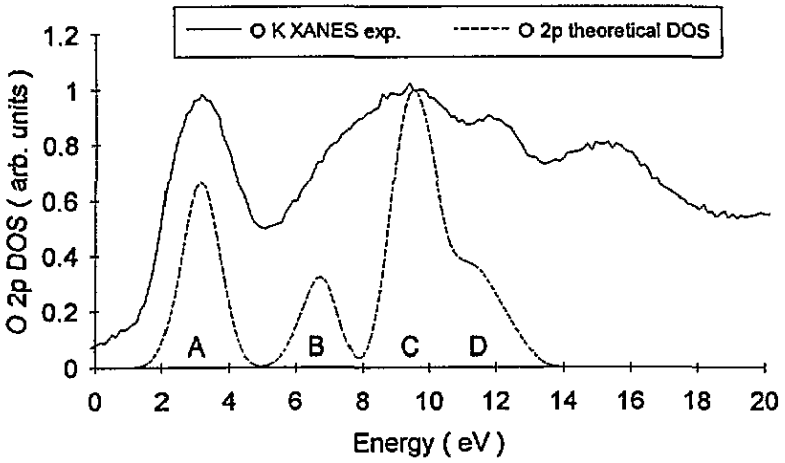

A	B	C	D
(O 2p, Nb 4d t_{2g}) π^*	(O 2p, Nb 4d e_g) σ^* (O 2p, Nb 5p) σ^* π^* (O 2p, Nb 5s) σ^*	(O 2p, Nb 5p) σ^* π^* (O 2p, Nb 4d e_g) σ^*	(O 2p, Nb 5s) σ^*

Figure 8. The O 2p theoretical DOS projection for cubic $KNbO_3$, in comparison with the experimental O K XANES spectrum of orthorhombic $KNbO_3$. Interpretations of XANES structures (A, B, C, D) are proposed in terms of (O 2p, Nb) orbital hybridizations.

Both structures B and C, observed respectively at 536 eV and 538.5 eV, are attributed to hybridization of O 2p orbitals with Nb 4d e_g (σ^* interaction) and Nb 5p (π^*, σ^* interactions). In addition, comparison of the partial DOS suggests a slight contribution of Nb 5s orbitals in shoulder B (σ^* interaction).

States due to hybridization occurring between O 2p and Nb 5s orbitals (σ^* interaction) take place beyond structure C, that is beyond Nb 5p. This latter hybridization could interpret structure D (540.7 eV), but this has to be ascertained with a greater atomic orbital basis.

Thus theoretical CB tight-binding calculations are in reasonable qualitative agreement with O K XANES experiments. Existing differences are understandable, when considering in particular the limited size of the atomic orbital basis and the non-consideration of the core-hole effect.

4.4. Nb L_1-edge XANES results

For the Nb L_1 edge, the final states are states of p symmetry (Nb 2s → Nb *n*p transitions). Comparison between the experimental Nb L_1 XANES spectrum (figure 4(*a*)) and the Nb 5p DOS calculation (figure 9) shows no straightforward structure assignment. Such discrepancies are particularly understandable when considering the atomic orbital basis extension. The atomic orbital basis is too short and also not convenient for the Nb L_1 edge. To take into account hybridizations of the Nb 5p orbitals, one has to increase the basis size.

4.5. K K-edge XANES results

For the K K-edge (figure 5), no XANES structure assignment can be given, since hybridizations of K orbitals were not considered during tight-binding calculations.

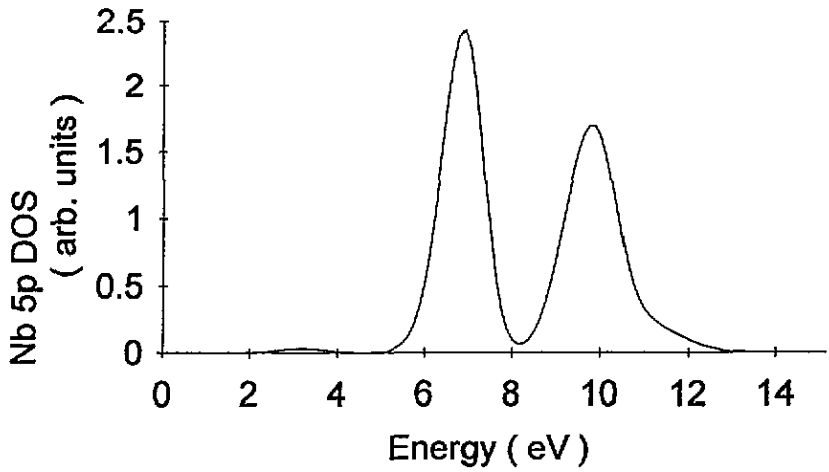

Figure 9. The Nb 5p theoretical DOS projection for cubic $KNbO_3$.

4.6. Charge distribution

Table 8 reports a recent theoretical charge distribution for $KNbO_3$. Large discrepancies exist between LMTO [6] and tight-binding [4, present work] results. The LMTO charge distribution seems particularly suspect since it gives a negative charge to the known electropositive K ion and a positive charge to the known electronegative O ions. Such discrepancies are probably due to the methods themselves. For instance, Neumann *et al* [6] suggest that the LMTO charge distribution may be simplified by the use of the atomic sphere approximation [23] and the choice of muffin-tin radii. However, comparison of theoretical charge distributions with a typical formal ionic charge distribution for a perovskite structure $K^{+}Nb^{5+}O_3^{2-}$ always suggests a significant hybridization of Nb 4d and O 2p states. This latter result is consistent with ^{93}Nb nuclear-resonance experiments by Cotts and Knight [24].

Table 8. Theoretical charge distributions.

Reference	K	Nb	O	Method
[6]	−0.83	+0.63	+0.07	LMTO
Present work	+1	1.80	−0.93	LCAO
[4]	+1	3.06	−1.35	LCAO
	+1	+5	−2	ionic model

5. Conclusion

We have probed orthorhombic $KNbO_3$ empty states by XANES spectroscopy, recorded at the O K edge, Nb L_1, L_2, and L_3 edges, and K K edge. Using tight-binding DOS calculations, XANES spectra were qualitatively interpreted in terms of orbital hybridizations. O K-edge structures are related to hybridizations of O 2p orbitals with 4d, 5p, and 5s Nb orbitals respectively. The Nb L_2 and L_3 edges reflect the (t_{2g}, e_g) degeneracy lift of the Nb 4d orbitals placed in an NbO_6 environment. Note that Nb 4d e_g states do not present a delocalized character significantly larger than that of t_{2g} states. More complete DOS calculations, taking

into account core-hole and spin–orbit coupling effects, are now in progress to ascertain XANES interpretations.

Acknowledgments

J Godard (Université Paris-Sud, Orsay) is acknowledged for the preparation of $KNbO_3$ monocrystals. The authors are grateful to P Lagarde, A M Flanck and G Tourillon from LURE (Orsay) for their XAS experimental support.

References

[1] Lines M E and Glass A M 1977 *Principles and Applications of Ferroelectrics and Related Materials* (Oxford: Oxford University Press)
[2] Fridkin V M 1979 *Photoferroelectrics* (Berlin: Springer)
[3] Pertosa P and Michel-Calendini F M 1978 *Phys. Rev.* B **17** 2011
[4] Castet-Mejean L and Michel-Calendini F M 1978 *J. Phys. C: Solid State Phys.* **11** 2195
Castet-Mejean L 1986 *J. Phys. C: Solid State Phys.* **19** 1637; 1991 *Phase Transitions* **36** 3
[5] Yong-Nian Xu, Ching W Y and French R H 1990 *Ferroelectrics* **111** 23
[6] Neumann T, Borstel G, Scharfschwerdt C and Neumann M 1992 *Phys. Rev.* B **46** 10623
[7] Soldatov A V, Sukhetskii Yu V, Ivantsov A A, Gusatinskii A N, Raevskii I P, Gubskii A L and Lisitsina S O 1988 *Ferroelectrics* **83** 193
[8] Hewat A W 1973 *J. Phys. C: Solid State Phys.* **6** 2559
[9] Wiesendanger E 1974 *Ferroelectrics* **6** 263
[10] Müller J E and Wilkins J W 1984 *Phys. Rev.* B **29** 4331
[11] Stöhr J 1988 *X-ray Absorption. Principles, Applications, Techniques of EXAFS, SEXAFS and XANES* ed D C Koningsberger and R Prins (New York: Wiley–Interscience) p 443
[12] Pettifer R F, Brouder C, Benfatto M, Natoli C R, Hermes C and Ruis López M F 1990 *Phys. Rev.* B **42** 37
[13] Harrison W A 1980 *Electronic Structure and Properties of Solids* (San Francisco: Freeman); 1981 *Phys. Rev.* B **24** 5835; 1985 *Phys. Rev.* B **31** 2121
[14] Jollet F and Noguera C 1993 *Phys. Status Solidi* b **179** 473
[15] Slater J C and Koster G F 1954 *Phys. Rev.* **94** 1498
[16] Lefebvre I, Lanoo M, Allan G and Martinage L 1988 *Phys. Rev.* B **38** 8593
Majewski J A and Vogl P 1986 *Phys. Rev. Lett.* **57** 1366
Chadi J C 1984 *Phys. Rev.* B **29** 785
[17] Jollet F, Noguera C, Thromat N, Gautier M and Duraud J P 1990 *Phys. Rev.* B **42** 7587
[18] Moore C E 1971 *NBS Circular* 467
[19] Michel-Calendini F M and Chermette H 1981 *J. Phys. C: Solid State Phys.* **14** 1179; 1980 *Ferroelectrics* **25** 495
[20] Yeh J J 1992 *Atomic Calculation of Photoionization Cross-Sections and Asymmetry Parameters* (London: Gordon and Breach) pp 31 and 97
[21] McGuire E J *Atomic Subshell Photoionization Cross Sections for* $2 \leqslant Z \leqslant 54$ SC-RR-70-721 (Albuquerque, NM: Sandia Laboratories) pp 14 and 51
[22] Teo B K and Lee P A 1979 *J. Am. Chem. Soc.* **101** 2815
[23] Andersen O K 1975 *Phys. Rev.* B **12** 3060
[24] Cotts R M and Knight W D 1954 *Phys. Rev.* **96** 1285